# IRON FLUORESCENT LINE EMISSION FROM YOUNG STELLAR OBJECTS IN THE ORION NEBULA

M. Tsujimoto,[1] E. D. Feigelson,[1] N. Grosso,[2] G. Micela,[3] Y. Tsuboi,[4] F. Favata,[5] H. Shang,[6] and J. H. Kastner[7]

## ABSTRACT

We present the result of a systematic search for the iron K$\alpha$ fluorescent line at $\sim$6.4 keV among 1616 X-ray sources detected by ultradeep *Chandra* observations of the Orion Nebula Cluster and the obscured Orion Molecular Cloud 1 population as part of the *Chandra* Orion Ultradeep Project (COUP). Seven sources are identified to have an excess emission at $\sim$6.4 keV among 127 control sample sources with significant counts in the 6.0–9.0 keV band. These seven sources are young stellar objects (YSOs) characterized by intense flarelike flux variations, thermal spectra, and near-infrared (NIR) counterparts. The observed equivalent widths of the line cannot be attributed to the florescence by interstellar or circumstellar matter along the line of sight. The X-ray spectral fits and NIR colors of the 6.4 keV sources show that these sources have X-ray absorption of $\gtrsim 1 \times 10^{22}$ cm$^{-2}$ and NIR excess emission, which is not expected when the fluorescence occurs at the stellar photosphere. We therefore conclude that the iron fluorescent line of YSOs arises from reflection off of circumstellar disks, which are irradiated by the hard X-ray continuum emission of magnetic reconnection flares.

*Subject headings:* ISM: individual (OMC-1) — open clusters and associations: individual (Orion Nebula Cluster) — scattering — stars: pre–main-sequence — X-rays: stars

## 1. INTRODUCTION

Contrary to most X-ray emission lines that convey information of "hot" celestial objects, fluorescent emission carries information of "cold" matter in the vicinity of bright X-ray sources. For a wide range of incident X-ray spectra, iron is the most visible element in the K fluorescent lines from the photoionized matter when its cosmic abundance and fluorescence yield are taken into account (George & Fabian 1991). The K$\alpha$ fluorescent line from neutral to low-ionized irons at $\sim$6.4 keV can be distinguished from K$\alpha$ lines from highly ionized irons ($\sim$6.7 keV by Fe xxv and $\sim$6.9 keV by Fe xxvi) using X-ray charge-coupled device (CCD) spectroscopy with a resolution of $\sim$150 eV at $\sim$6 keV. The line can also penetrate through a large column density up to a few times $10^{24}$ cm$^{-2}$, which gives the opacity $\tau = 1$ by photoelectric absorption. All these features make iron K$\alpha$ fluorescence a unique observational tool to investigate the environment in which the continuum X-ray sources reside.

The fluorescent line is reported in a variety of X-ray emitters. The two most widely known classes are X-ray binaries and active galactic nuclei (AGNs). The detections of the line also extend to giant molecular clouds (e.g., Sgr B2; Koyama et al. 1996b), massive stars (e.g., $\eta$ Car; Corcoran et al. 1998), supernova remnants (e.g., RCW 86; Vink et al. 1997), and unidentified sources in the Galactic center (Park et al. 2004). In $\eta$ Car, Corcoran et al. (1998) attributed the line to the fluorescence from photoionized circumstellar matter along the line of sight.

The best-studied case of this emission is the Sun. The 6.4 keV line was first discovered during solar flares (Neupert et al. 1967). Subsequent studies revealed that the photoionization by flare X-rays is more likely to produce this line than collision ionization by accelerated particles (Doschek et al. 1971). Parmar et al. (1984) made a systematic survey of the 6.4 keV emission among $\sim$600 solar flares detected by the *Solar Maximum Mission*. Their result was consistent with the calculation by Bai (1979), who made a model assuming that the 6.4 keV line is iron fluorescence at the solar photosphere.

Recently, Imanishi et al. (2001) detected the line emission from a class I protostar in $\rho$ Ophiuchi dark cloud at $\sim$145 pc (de Zeeuw et al. 1999) with *Chandra*. The protostar YLW 16A produced a huge flare during the observation reaching a luminosity of $1.4 \times 10^{32}$ ergs s$^{-1}$ (0.5–9.0 keV), during which a 6.4 keV line emerged in its X-ray spectrum with an equivalent width (EW) of $\lesssim$180 eV. They interpreted that the emission is from a face-on protostellar disk irradiated by the intense X-rays from a magnetic reconnection event. The previous *ASCA* detection of a $\sim$6.2 keV emission line from an embedded far-infrared source in the R CrA cluster (Koyama et al. 1996b) might be another example. These detections point out the potential importance of this X-ray line to diagnose deeply embedded protostars and their surroundings, although the geometry of the reflection for the fluorescence is not certain with only a few detections. Continuum sources are presumably flare X-rays, but reflectors can be interstellar matter along the line of sight, disks, or photosphere. Systematic studies with more samples are mandatory to elucidate the general picture of this faint emission.

This paper has two purposes: (1) to establish the presence of the iron fluorescent line from young stellar objects (YSOs) with a larger number of detections and (2) to examine the geometry of reflection by comparing the 6.4 keV sample to a control sample not showing the line. We utilize the most sensitive X-ray observation ever obtained of a star-forming region, the *Chandra* Orion Ultradeep Project (COUP),[8] to conduct a systematic search

[1] Department of Astronomy and Astrophysics, The Pennsylvania State University, 525 Davey Laboratory, University Park, PA 16802.

[2] Laboratoire d'Astrophysique de Grenoble, 414 rue de la Piscine, Université Joseph-Fourier BP 53, 38041 Grenoble cedex 9, France.

[3] INAF, Osservatorio Astronomico di Palermo, Piazza del Parlamento 1, 90134 Palermo, Italy.

[4] Department of Physics, Chuo University, Kasuga 1-13-27, Bunkyo-ku, Tokyo 112-8551, Japan.

[5] Astrophysics Division, Research and Science Support Department of ESA, ESTEC, Postbus 299, 2200 AG Noordwijk, Netherlands.

[6] Institute of Astronomy and Astrophysics, Academia Sinica, Taipei 106, Taiwan.

[7] Center for Imaging Science, Rochester Institute of Technology, Rochester, NY 14623.

[8] Links to the COUP data set are available in the electronic edition of the *Supplement*.

for sources with an excess emission at $\sim$6.4 keV. We report the detections of seven YSOs with the iron fluorescent line and present the interpretation that these fluorescent lines occur following irradiation of disks by intense flare X-rays.

## 2. OBSERVATION AND DATA REDUCTION

The COUP observations were carried out in 2003 January for 13 consecutive days with a total exposure time of $\sim$838 ks. The ACIS (Advanced CCD Imaging Spectrometer; Garmire et al. 2003) instrument on board *Chandra* (Weisskopf et al. 2002) was used to take an X-ray image covering a $17' \times 17'$ region in the Orion Nebula Cluster (ONC) at a distance of $\sim$450 pc (Genzel & Stutzki 1989). The image was centered at R.A. = $5^h35^m17^s$ and decl. = $-5°23'40''$ (J2000.0) to cover the entire ONC and its vicinity, including the Orion Molecular Cloud 1 cores. The data were taken with the very faint telemetry mode and the timed exposure CCD operation with a frame time of 3.2 s.

Details of the data reduction are described in Getman et al. (2005). Briefly, after removing non–X-ray events and correcting for charge transfer inefficiency, a source search was performed to detect 1616 X-ray sources. They were matched with various optical and near-infrared (NIR) catalogs for identification. X-ray events of each source were accumulated from an $\sim$87% encircled energy polygon at the source position. Consistent imaging, spectral, and timing analyses were conducted for all sources. In the spectral analysis, 0.5–8.0 keV spectra were fitted by a thin-thermal plasma model (MEKAL; Mewe et al. 1985; Liedahl et al. 1995) with interstellar absorption (wabs), varying X-ray luminosity ($L_X$), plasma temperature ($k_BT$), and equivalent hydrogen column density ($N_H$) values. When a large residual was found, another temperature component was added to improve the fits.

## 3. SEARCH FOR FLUORESCENT LINE EMISSION

### 3.1. *Control Sample and Event Extraction*

Among the 1616 COUP sources, we first define a control sample to search for the 6.4 keV emission, which is restricted to sufficiently bright and spectrally hard sources. We set two criteria of >100 photons and signal-to-noise ratio of >20 in the 6.0–9.0 keV band to obtain a sample consisting of 127 sources. Here we used a maximum energy of 9.0 keV rather than the 8.0 keV used by Getman et al. (2005) to better determine the continuum level beyond the iron K$\alpha$ lines at 6.4–6.9 keV.

Forty-nine of these 127 sources have a "p" flag in the COUP source list (Getman et al. 2005), indicating that they are possibly piled up. We developed a method for pile-up mitigation based on photon extraction in an annulus around the pile-up core of the point-spread function.[9] We accumulate X-ray events from an $\sim$87% encircled energy polygon with the central circular core removed. We derive an energy-dependent correction to the auxiliary response file for the annular region based on simulations using the ChaRT and MARX software packages.[10] The correction function is a low-order polynomial that does not introduce artificial features in the corrected effective area function. Unlike the method by Davis (2001), which is restricted to mildly piled-up sources, our procedure is successfully applied to both mildly and severely piled-up sources. Events extracted from the annular

regions were confirmed to meet the criteria for the control sample.

### 3.2. *Spectral Fitting*

For the 127 hard and bright COUP sources, 44 were successfully fitted with one-temperature thermal models and 83 were fitted with two-temperature models, following the procedure given by Getman et al. (2005). We made fits in the 2.0–9.0 keV band with $N_H$ fixed to the values tabulated by Getman et al. (2005). The iron metallicity value was treated as a free parameter, while the metallicity of other elements was left fixed to 0.3 solar.

We added onto the best-fit plasma model a Gaussian line component at 6.40 keV with the intrinsic width fixed to 0 and a free normalization ($N_{K\alpha}$). Here 6.40 keV is the weighted mean of two unresolved K$\alpha$ fluorescent lines from neutral irons at 6.391 and 6.404 keV (K$\alpha_1$ and K$\alpha_2$; George & Fabian 1991). The energy shift of the line center due to ions at different ionization stages makes a negligible contribution with $\lesssim$1% for neutral to low-ionized irons (Fe I–Fe IX; House 1969). The intrinsic width of these lines ($\sim$0.4 eV and $\sim$3.5 eV for thermal and quantum broadenings; George & Fabian 1991) and the width by the blending ($\sim$12 eV) are both negligible compared to the energy resolution of the detector ($\sim$150 eV). We derive $N_{K\alpha}$, the EW of the line (EW$_{K\alpha}$), and the null hypothesis probability of the $F$-test ($P_F$) to examine whether an additional model is statistically justified. With a careful inspection of the result, we recognized spectra to have a 6.4 keV feature when (1) the 90% lower limit of $N_{K\alpha}$ exceeds 0 and (2) $P_F$ is less than 1%. This suppresses the number of false positives to be $\sim$1. We further removed manually a few suspicious sources that satisfied these criteria but did not visually show convincing fluorescent line emission; these sources are piled-up sources that have distorted spectra even in reduced event accumulation regions.

This procedure produces seven positive fluorescent line detections out of the 127 sources. Table 1 lists the name, the COUP sequence number, and the best-fit values both of the Gaussian and thermal spectral components of the seven sources, while the spectra of these sources are displayed in Figure 1.

### 3.3. *Light Curves*

The light curves were constructed for all the control sample sources using events in the 2.0–9.0 keV band and were segmented into pieces with a constant flux using a Bayesian block algorithm (Scargle 1998). The details on the application of algorithm to the COUP data are given in Getman et al. (2005).

The light curves of the seven 6.4 keV sources are given in Figure 2. Time-sliced spectroscopy of these seven sources is not feasible because of the paucity of the signal. We also checked the previous two short ACIS observations of the ONC (Feigelson et al. 2002) and found none of these sources have enough counts for a similar analysis.

### 3.4. *Stellar Counterparts of the Control Sample Sources*

Most of the 1616 COUP sources, thus most of the control sample sources, are YSOs that belong to Orion Nebula population. However, a significant contamination comes from background AGNs. We estimate no more than $\approx$6 AGNs in the control sample based on the following calculation. The threshold of the control sample of 100 counts in the 6.0–9.0 keV band is converted to an X-ray flux of $\sim$3.3 $\times$ $10^{-14}$ ergs s$^{-1}$ cm$^{-2}$ (2.0–7.0 keV) assuming a power-law spectrum of an index typical of

---

[9] More details are given by Getman et al. (2005) and at http://www.astro.psu.edu/users/tsujimot/arfcorr.html.

[10] See http://asc.harvard.edu/chart/ and http://space.mit.edu/CXC/MARX/.

TABLE 1
X-Ray Fitting Result of 6.4 keV Sources

| Number[a] | Name | COUP[b] Sequence Number | NetCts[c] | $N_{\mathrm{K}\alpha}$[d,e] $(10^{-7}\ \mathrm{cm}^{-2}\ \mathrm{s}^{-1})$ | $\mathrm{EW}_{\mathrm{K}\alpha}$[e] (eV) | $P_F$[e] $(10^{-3})$ | $N_{\mathrm{H}}$[f] $(10^{22}\ \mathrm{cm}^{-2})$ | $k_{\mathrm{B}}T$[d,f] (keV) | $L_{\mathrm{X}}$[d,f] $(10^{30}\ \mathrm{ergs}\ \mathrm{s}^{-1})$ | $L_{\mathrm{X, peak}}$[g] $(10^{31}\ \mathrm{ergs}\ \mathrm{s}^{-1})$ |
|---|---|---|---|---|---|---|---|---|---|---|
| 1............ | 053509.2−053058 | 331 | 268 | 2.6 (0.1–4.6) | 126 | 5.6 | 1.58 | 4.6 (4.3–5.6) | 3.4 (2.7–3.9) | 17 |
| 2............ | 053513.6−051954 | 561 | 332 | 3.6 (1.1–7.3) | 130 | 0.8 | 1.45 | 2.8 (2.6–2.9) | 5.6 (5.8–6.1) | 4.4 |
| 3............ | 053514.3−052232 | 621 | 304 | 2.5 (0.5–3.9) | 111 | 6.2 | 5.62 | 3.2 (2.9–3.4) | 4.1 (3.4–4.8) | 1.6 |
| 4............ | 053514.6−052211 | 647 | 272 | 4.1 (1.9–6.2) | 135 | 5.7 | 30.9 | 5.7 (4.7–8.1) | 3.3 (2.9–4.1) | 5.7 |
| 5............ | 053514.6−052301 | 649 | 107 | 1.2 (0.3–2.2) | 268 | 6.4 | 0.93 | 3.0 (2.6–3.1) | 1.4 (1.0–1.7) | 2.1 |
| 6†.......... | 053519.3−052542 | 1030 | 461 | 17 (2.5–17) | 111 | 5.9 | 11.5 | 9.4 (6.4–14) | 11 (9.3–12) | 45 |
| 7............ | 053519.6−051326 | 1040 | 266 | 4.3 (1.5–6.6) | 122 | 6.0 | 1.91 | 3.3 (3.0–3.5) | 6.7 (6.2–7.2) | 40 |

[a] Piled-up source for which we applied our pile-up mitigation method is marked with a dagger (†).
[b] Sequence number of the COUP sources (Getman et al. 2005).
[c] Counts in the 6.0–9.0 keV range. For the pile-up source, counts in the annulus region is given.
[d] The 90% uncertainty is given in parentheses.
[e] The fitting result of the additional 6.4 keV Gaussian to the best-fit thin-thermal plasma model.
[f] The fitting result of the thin-thermal plasma model. For two-temperature spectra, the values of the higher temperature component are given.
[g] The peak X-ray luminosity during the flares. The values were derived from the maximum and average count rates among segmented blocks assuming no spectral change.

AGNs ($-1.7$) absorbed with a column density of $10^{22}\ \mathrm{cm}^{-2}$, as a rough estimate of the averaged value in the COUP field. Using

$$N(>S) = 1200\left(\frac{S}{2\times10^{-15}\ \mathrm{ergs\ s^{-1}\ cm^{-2}}}\right)^{-1.0} \quad (1)$$

from Giacconi et al. (2001), where $N\ (>S)$ is the number of background X-ray sources per square degree brighter than $S$ ergs s$^{-1}$, no more than $\approx 6$ AGNs are expected above the 100 count threshold. We believe four of these AGN sources can be identified: COUP sequence numbers 8, 723, 1053, and 1304 (Getman et al. 2005). They exhibit no flarelike flux variations, show no spectral lines, and have best-fit $k_{\mathrm{B}}T$ above 15 keV. Unphysically high temperature values are often introduced by fitting a flat power-law spectrum with a thermal model. We are thus confident that the remaining 123 sources are Orion population members and consider them to be the control sample hereafter.

The seven sources with the 6.4 keV feature clearly have YSO properties: 6.7 keV line emission arising from the K$\alpha$ line of Fe xxv (Fig. 1), light curves showing high-amplitude flux variation typical of YSO flares (Fig. 2), and NIR identifications except for number 4 (Table 2). The lack of a NIR counterpart for number 4 is probably due to an exceptionally high column density exceeding $3\times10^{23}\ \mathrm{cm}^{-2}$ (Table 1).

## 4. DISCUSSION

We have now established that seven of 123 hard and bright COUP stellar X-ray sources show 6.4 keV line emission. All of them exhibit powerful X-ray flares and thermal plasma line emission typical of YSOs. Most of them also have NIR photospheric counterparts. We now proceed to make inferences about these sources concerning the nature of these stars and the origin of the fluorescent line emission.

### 4.1. Location of the Fluorescing Material

The observed EW values give us a constraint on the geometry of the continuum source and the reflector that gives rise to the fluorescence. The following calculation demonstrates the improbability that the fluorescent line arises in circumstellar or interstellar matter along the line of sight of the continuum X-rays.

EW values of the K$\alpha$ fluorescent line are related to the incident hot continuum and ambient cold material as (Liedahl 1998)

$$\mathrm{EW}_{\mathrm{K}\alpha} = \frac{L_{\mathrm{K}\alpha}}{I(E_{\mathrm{K}\alpha})} = \left(\frac{\Delta\Omega}{4\pi}\right)Y_{\mathrm{K}\alpha}\frac{E_{\mathrm{K}\alpha}}{I(E_{\mathrm{K}\alpha})}$$
$$\times \int n_{\mathrm{Fe}}(s)\,ds \int_{\chi}^{\infty}\frac{I(E')}{E'}\sigma_{\mathrm{Fe}}(E')\,dE'. \quad (2)$$

Here we suppose that the incident X-ray with a spectrum of $I(E)$ is photoelectrically absorbed by a reflector that subtends the angle $\Delta\Omega$ seen from the continuum source. The reflector, which is assumed to be optically thin to hard X-rays, has an iron density of $n_{\mathrm{Fe}}(s)$ along the line of ray ($s$) with the photoelectric cross section of $\sigma_{\mathrm{Fe}}(E)$. The energy integral begins at the iron K edge energy $\chi$. The K$\alpha$ fluorescent line with the luminosity $L_{\mathrm{K}\alpha}$ is subsequently emitted at the energy $E_{\mathrm{K}\alpha}$ with a fluorescence yield of $Y_{\mathrm{K}\alpha}$. Assuming a thermal bremsstrahlung spectrum for the continuum source; $I(E) \propto \exp(-E/k_{\mathrm{B}}T)$ and $\sigma_{\mathrm{Fe}}(E) = (E/\chi)^{-3}\sigma_{\mathrm{Fe}}(\chi)$, we obtain

$$\mathrm{EW}_{\mathrm{K}\alpha} = \left(\frac{\Delta\Omega}{4\pi}\right)Y_{\mathrm{K}\alpha}E_{\mathrm{K}\alpha}N'_{\mathrm{H}}Z_{\mathrm{Fe}}\sigma_{\mathrm{Fe}}(\chi)$$
$$\times \exp\left(\frac{E_{\mathrm{K}\alpha}}{k_{\mathrm{B}}T}\right)\left(\frac{k_{\mathrm{B}}T}{\chi}\right)^{-3}\int_{\chi/k_{\mathrm{B}}T}^{\infty}\exp(-x)x^{-4}\,dx. \quad (3)$$

The integral along $s$ is converted to an equivalent hydrogen column density $[N'_{\mathrm{H}} = \int n_{\mathrm{H}}(s)\,ds]$ using $n_{\mathrm{Fe}}(s) = Z_{\mathrm{Fe}}n_{\mathrm{H}}(s)$, where $n_{\mathrm{H}}(s)$ is the hydrogen density and $Z_{\mathrm{Fe}}$ is the elemental abundance of iron relative to hydrogen in the reflector. Substituting $Y_{\mathrm{K}\alpha} = 0.34$ (Kortright 2001), $E_{\mathrm{K}\alpha} = 6.40$ keV, $\chi = 7.11$ keV, $\sigma_{\mathrm{Fe}}(\chi) = 2\times10^{-20}\ \mathrm{cm}^{-2}$ (Gullikson 2001), and $Z_{\mathrm{Fe}} = 3\times10^{-5}$ (Däppen 2000), $\mathrm{EW}_{\mathrm{K}\alpha}$ is evaluated as

$$\mathrm{EW}_{\mathrm{K}\alpha} = \alpha\left(\frac{\Delta\Omega}{4\pi}\right)\left(\frac{N'_{\mathrm{H}}}{10^{22}\ \mathrm{cm}^{-2}}\right)\ \mathrm{eV}, \quad (4)$$

where $\alpha$ is a constant that has a weak dependence on $k_{\mathrm{B}}T$. Between 3 and 10 keV in which our 6.4 keV sample sources are distributed (Table 1), $\alpha$ has an approximate value of $\sim 2.5$ (1.8–3.1). The value is slightly smaller than the one ($\sim 3.3$) calculated for Seyfert galaxies with a power-law incident spectrum of
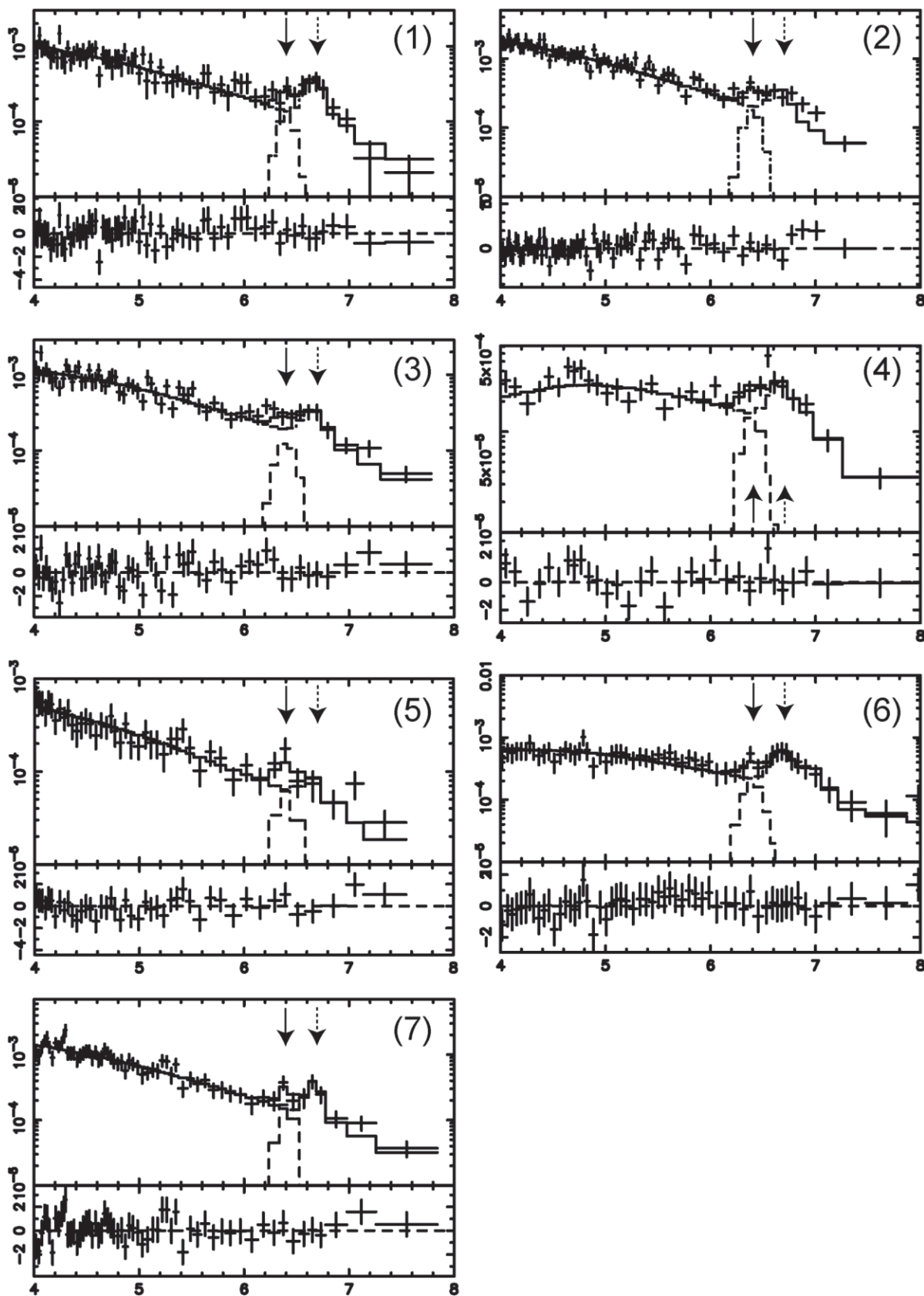
Fig. 1.—Spectra and best-fit models of 6.4 keV sources. The upper panels show the spectra ( *plus signs*) and the best-fit models (*solid steps*) with a Gaussian component shown by dashed steps. The 6.4 and 6.7 keV lines are indicated by solid and dashed arrows, respectively. The abscissa is the energy from 4.0 to 8.0 keV, while the ordinate is the spectral intensity in the unit of counts s$^{-1}$ keV$^{-1}$. The lower panels show the residual to the fit, where the ordinate shows $\chi$-values of each bin.
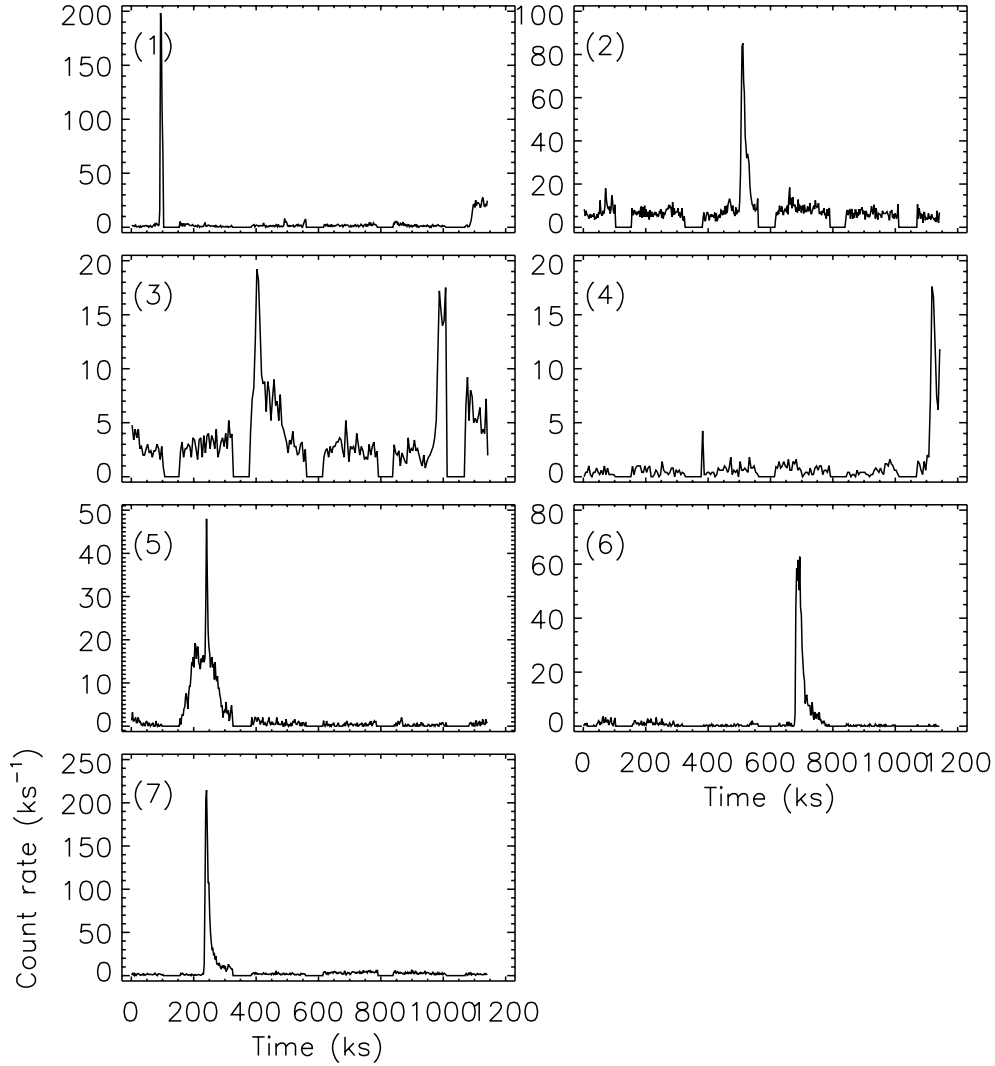
FIG. 2.—Light curves of 6.4 keV sources in 2.0–9.0 keV band. The abscissa is the time from the start of the observation, while the ordinate is the detector count rate of each time bin. The light curves are binned with 2500 or 5000 s bin$^{-1}$ according to their brightness.

TABLE 2
NIR COLORS OF 6.4 keV SOURCES

| Number | $JHK_s$[a] Counterparts | $J$ (mag) | $H$ (mag) | $K_s$ (mag) | $L'$[b] Counterparts | $L'$ (mag) | TPSC[c] |
|---|---|---|---|---|---|---|---|
| 1...................... | 05350920−0530585† | 12.5 | 10.6 | 9.4 | . . . | . . . | . . . |
| 2...................... | 387 | 11.1 | 9.4 | 8.3 | 1007 | 6.7 | 18 |
| 3...................... | 428 | 14.9 | 11.3 | 8.6 | 598 | 5.7 | 43 |
| 4...................... | . . . | . . . | . . . | . . . | . . . | . . . | . . . |
| 5...................... | 446 | 12.6 | 11.4 | 10.8 | 175‡ | 10.5 | . . . |
| 6...................... | 801 | 16.0 | 12.4 | 9.9 | 42 | 7.4 | 41 |
| 7...................... | 05351965−0513264† | 14.0 | 11.5 | 10.2 | . . . | . . . | . . . |

[a] $J$, $H$, and $K_s$ magnitudes are either from the 2MASS all-sky survey catalog (†) or M. J. McCaughrean et al. (2005, in preparation).
[b] $L'$ magnitudes are either from Muench et al. (2002) or Lada et al. (2004) (‡). Numbers 1 and 7 are located outside the $L'$-band surveys.
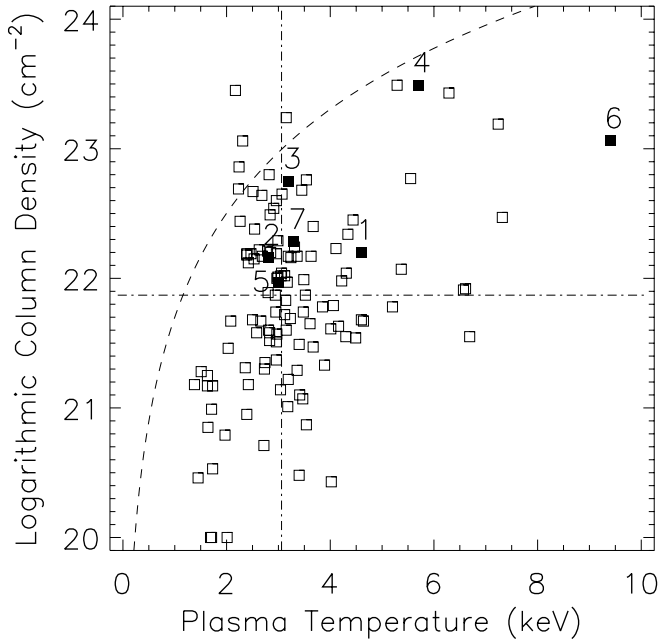[c] Numbers of the protostar candidate sources listed in Lada et al. (2000).

Fig. 3.—Scatter plot of plasma temperature and column density of the control sample (*squares*). Sources with the 6.4 keV feature are marked filled with their source numbers. The dash-dotted lines indicate the median values of $N_H$ and $k_B T$ of the control sample. The dotted curve is the column density to have the opacity $\tau = 1$ to the X-rays at a given temperature, which roughly indicates the observational bias.

$I(E) \propto (E/\chi)^{-0.7}$ (e.g., Krolik & Kallman 1987), reflecting the exponential cutoff of thermal spectra at the hard end.

If the fluorescence is caused by circumstellar or interstellar matter along the line of sight of the continuum X-rays, the $N'_H$-values would be the same with $N_H$ derived from the X-ray spectral fits (Table 1). This can account for only a few percent of the observed EW values as $\Delta\Omega/4\pi \leq 1$ (eq. [4]). A geometry is

thus required in which the photoionizing X-rays suffer a localized absorption much larger than that in the line of sight. This is consistent with the result by Imanishi et al. (2001) concerning YLW 16A, where they set an upper limit of ~20 AU upon the distance from the protostar to the reflector, based on the lack of detectable time lag between the flare start and the appearance of the fluorescent emission.

### 4.2. *Absorption and NIR Colors of the Fluorescent X-Ray Sources*

Two conceivable geometries to realize localized reflection are (1) the reflection by the stellar photosphere like in the Sun; and (2) the reflection by a circumstellar structure like a disk. Our examination of the X-ray absorption and the NIR colors of the 6.4 keV sources in comparison with the control sample points to a circumstellar origin.

Figure 3 shows a scatter plot between $N_H$ and $k_B T$. The median value of $N_H$ among the 123 control sample sources is $10^{21.9}$ cm$^{-2}$. All of the 6.4 keV sources show larger absorption than this. The preference, which has a null hypothesis probability of ~0.8%, is not expected if the reflection occurs at photosphere. It would be likely, on the other hand, when the reflection takes place at disks, because YSOs with disks are younger in their evolution than those without disks and tend to have denser circumstellar matter yielding larger $N_H$.

Using $J$-, $H$-, $K_s$-, and $L'$-band magnitudes of the NIR counterparts for the control sample sources, we show color-color diagrams in Figure 4. The NIR identifications and magnitudes follow Getman et al. (2005). Among 123 YSO samples, 109 have significant $J$-, $H$-, and $K_s$-band detections and 66 additionally have significant $L'$-band detections to be plotted on the diagrams. The $(J - H)/(H - K_s)$ and $(H - K_s)/(K_s - L')$ diagrams (Figs. 4a and 4b) complement with each other, where the former covers fainter sources using shorter wavelength data, while the latter is more sensitive to cooler circumstellar matter by using longer wavelength data. At least four 6.4 keV sources
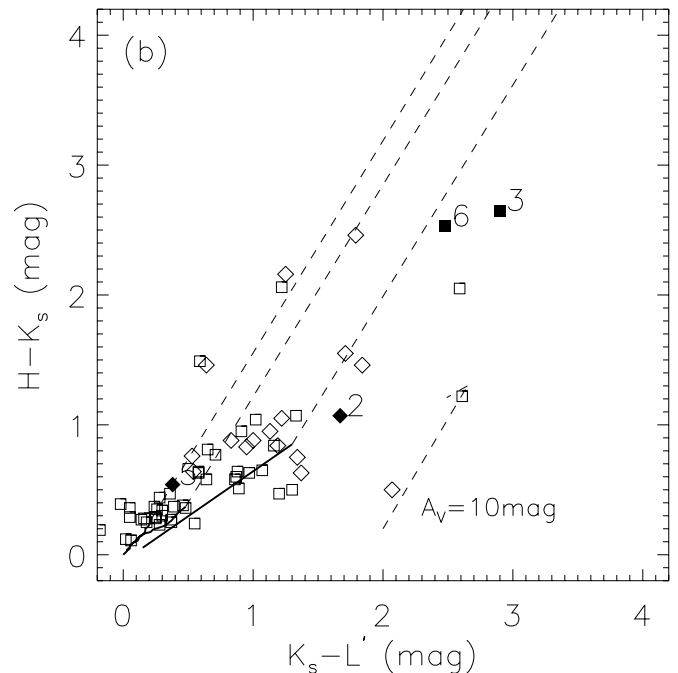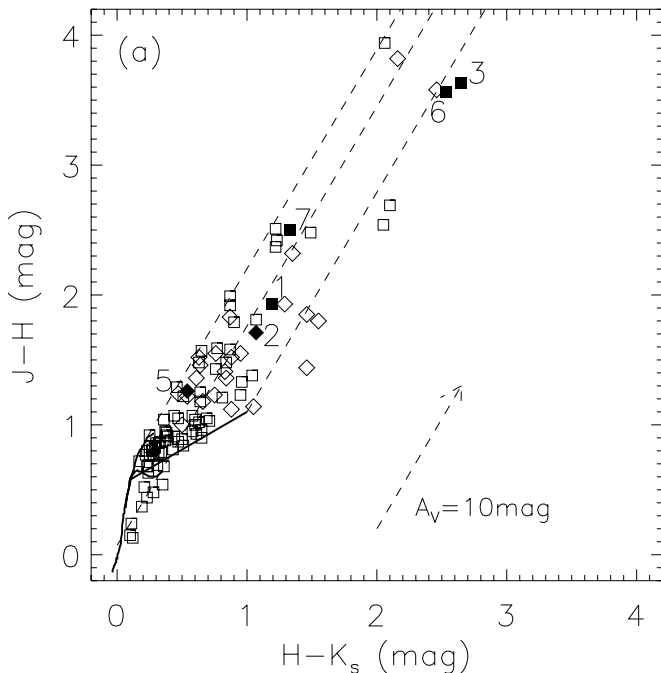


Fig. 4.—(a) $(J - H)/(H - K_s)$ and (b) $(H - K_s)/(K_s - L')$ diagrams of the control sample sources. Squares are for sources with larger $k_B T$ and $N_H$ than the medium values, while diamonds are for remainders. The 6.4 keV sources are marked filled with a label of their source numbers. The reddening lines are shown with dashed lines from the intrinsic colors of dwarfs and giants (*thick solid curves*; Tokunaga 2000) and the classical T Tauri star locus (*thick solid lines*; Meyer et al. 1997). No conversion of the color systems is made to the data.
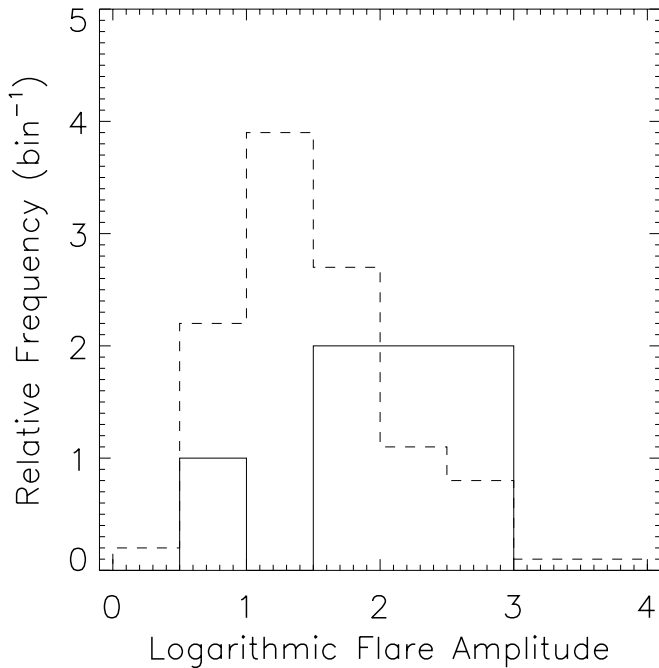
Fig. 5.—Histograms of flare amplitude for the 6.4 keV sources (*solid*) and the control sample sources (*dashed*). The frequency of the control sample sources is reduced by a factor of 10 to facilitate comparison.

(numbers 1, 2, 3, and 6) out of six with NIR counterparts lie outside the region of reddened dwarfs and giants, indicating the presence of NIR-emitting inner disks. The preference to have NIR excess emission is consistent the idea that fluorescent reflection occurs at disks.

### 4.3. *Fluorescence and Flares*

All of the 123 control sample sources have more than two Bayesian block segments, indicating flux variation. Most of them exhibit variation typical to flares with a fast rise and slow decay profile. All of the seven sources with iron fluorescence have large-amplitude flares (Fig. 2).

Our sample is heavily biased for flare sources. Therefore, we do not conclude that a flare is a required factor for fluorescence, despite the facts that all fluorescence sources exhibit flares and that we did not favor for flare sources in identifying the fluorescence line by fitting time-integrated spectra.

The flare amplitude, however, appears to be related to the fluorescence. Figure 5 shows the histograms of flare amplitude of the control sample and 6.4 keV sources, where we define the flare amplitude as the ratio between the maximum and the minimum count rates of all Bayesian block segments. Six out of seven 6.4 keV sources have larger amplitudes than the median value ($\sim 10^{1.42}$) among the control sample, making the null hypothesis probability of this preference to be $\sim 6\%$. Large-amplitude flares may have a preferable geometry for fluorescence to occur, which should be examined by future studies.

### 4.4. *Constraints on the Geometry of the Fluorescent Sources*

We consider that the lack of 6.4 keV detections from the other 116 sources is not completely attributable to a statistical inadequacy of the data. About 14% of the 116 YSO samples without a 6.4 keV detection show (1) $N_H$ and $k_B T$ larger than the median values and (2) significant NIR excess emission (Figs. 4a and 4b, *squares located to the right of the middle reddening lines*). Most of them have more counts in the 6–9 keV band than the weakest

of the seven 6.4 keV sources (107 counts for number 5; Table 1), which is close to the threshold for the control sample. The absence of the fluorescence line thus appears to be a physical not data-dependent statistical characteristic.

One idea is the disk orientation, if the fluorescence occurs at disks illuminated from atop (the lamppost geometry). The geometry is considered a likely explanation for the iron fluorescent emission from the accretion disks in Seyfert galaxies and X-ray binaries (Nayakshin & Kallman 2001). Face-on inclination is more favorable than edge-on inclination for the fluorescence X-rays to escape. George & Fabian (1991) presented a relation between the expected EW of the fluorescent line and the disk inclination with a radiative transfer treatment. The calculation assumed a configuration in which a continuum source is at a height of $0.01r$ above the center of a disk with a radius of $r$. The EW value decreases drastically for large inclination angles relative to the normal of the disk (see George & Fabian 1991, Fig. 14). It may be the case that the bright sources without a 6.4 keV detection have unfavorable inclination angles seen from us.

A simple consideration on the observed EW values also supports this picture. The iron fluorescence can come out from any depth from the surface of disks corresponding to different $N_H'$-values, but we speculate that the observed fluorescence is dominated by the light reflected at $N_H' \sim 10^{24}$ cm$^{-2}$, where 6.4 keV X-rays suffer photoelectric absorption of the opacity $\tau \lesssim 1$. We would expect a smaller EW$_{Fe}$ if $N_H'$ is smaller than $\sim 10^{24}$ cm$^{-2}$ by equation (4). The claim is also the case if $N_H'$ is larger, because the emitted 6.4 keV X-rays would be severely attenuated through the reflector (Makishima 1986). By substituting $N_H' \sim 10^{24}$ cm$^{-2}$ and EW$_{Fe} \sim 140$ eV, which is the mean value of all seven sources (Table 1), we can derive $(\Delta\Omega/4\pi) \sim 0.5$. This is consistent with the assumption that the disk is illuminated in a lamppost configuration to realize the subtended angle, and the disk is oriented face-on so that the fluorescent X-rays suffer no extra attenuation through the disk.

The detection of the 6.4 keV line has an astrophysical implication on X-ray ionization of disks. Many studies (e.g., Glassgold et al. 2000) have suggested that X-ray photoionization, in addition to cosmic-ray collision ionization, can be a dominant ionization source for circumstellar material around forming stars, which is an important process to couple the gas with the ambient magnetic field. Our detection of the recombination line at 6.4 keV is a direct observational proof that the X-ray photoionization does take place at disks.

Finally, we note that the reflection may occur in different disk geometries such as X-ray irradiation at the inner edge of the disk, or at other circumstellar structures such as funnel flow, jet, or wind columns; these structures are associated with sources at an early stage of YSO evolution. So far, we have no observational argument to distinguish among these possibilities. The measurement of the delay time from the onset of flares to the appearance of the 6.4 keV line, as was tried by Imanishi et al. (2001) for an upper limit value, will bring a key observational basis for future X-ray experiments such as *Constellation-X*.

*Facilities:* CXO (ACIS)

## REFERENCES

Bai, T. 1979, Sol. Phys., 62, 113
Corcoran, M. F., et al. 1998, ApJ, 494, 381
Däppen, W. 2000, in Allen's Astrophysical Quantities, ed. A. N. Cox (New York: Springer), 27
Davis, J. E. 2001, ApJ, 562, 575
de Zeeuw, P. T., Hoogerwerf, R., de Bruijne, J. H. J., Brown, A. G. A., & Blaauw, A. 1999, AJ, 117, 354
Doschek, G. A., Meekins, J. F., Kreplin, R. W., Chubb, T. A., & Friedman, H. 1971, ApJ, 170, 573
Feigelson, E. D., Broos, P., Gaffney, J. A., Garmire, G., Hillenbrand, L. A., Pravdo, S. H., Townsley, L., & Tsuboi, Y. 2002, ApJ, 574, 258
Garmire, G. P., Bautz, M. W., Ford, P. G., Nousek, J. A., & Ricker, G. R. 2003, Proc. SPIE, 4851, 28
Genzel, R., & Stutzki, J. 1989, ARA&A, 27, 41
George, I. M., & Fabian, A. C. 1991, MNRAS, 249, 352
Getman, K. V., et al. 2005, ApJS, 160, 319
Giacconi, R., et al. 2001, ApJ, 551, 624
Glassgold, A. E., Feigelson, E. D., & Montmerle, T. 2000, in Protostars and Planets IV, ed. V. Mannings, A. P. Boss, & S. S. Russell (Tucson: Univ. Arizona Press), 429
Gullikson, E. M. 2001, in X-Ray Data Booklet, ed. A. Thompson et al. (Berkeley: Univ. California), 38
House, L. L. 1969, ApJS, 18, 21
Imanishi, K., Koyama, K., & Tsuboi, Y. 2001, ApJ, 557, 747
Kortright, J. B. 2001, in X-Ray Data Booklet, ed. A. Thompson et al. (Berkeley: Univ. California), 28
Koyama, K., Maeda, Y., Sonobe, T., Takeshima, T., Tanaka, Y., & Yamauchi, S. 1996b, PASJ, 48, 249

Krolik, J. H., & Kallman, T. R. 1987, ApJ, 320, L5
Lada, C. J., Muench, A. A., Haisch, K. E., Lada, E. A., Alves, J. F., Tollestrup, E. V., & Willner, S. P. 2000, AJ, 120, 3162
Lada, C. J., Muench, A. A., Lada, E. A., & Alves, J. F. 2004, AJ, 128, 1254
Liedahl, D. A. 1998, in Lecture Notes in Phys. 520, X-Ray Spectroscopy in Astrophysics, ed. J. van Paradijs, & J. A. M. Bleeker (Berlin: Springer), 189
Liedahl, D. A., Osterheld, A. L., & Goldstein, W. H. 1995, ApJ, 438, L115
Makishima, K. 1986, in Lecture Notes in Phys. 266, The Physics of Accretion onto Compact Objects, ed. K. O Mason, M. G. Watson, & N. E. White (Berlin: Springer), 249
Mewe, R., Gronenschild, E. H. B. M., & van den Oord, G. H. J. 1985, A&AS, 62, 197
Meyer, M. R., Calvet, N., & Hillenbrand, L. A. 1997, AJ, 114, 288
Muench, A. A., Lada, E. A., Lada, C. J., & Alves, J. 2002, ApJ, 573, 366
Nayakshin, S., & Kallman, T. R. 2001, ApJ, 546, 406
Neupert, W. M., Gates, W., Swartz, M., & Young, R. 1967, ApJ, 149, L79
Park, S., Muno, M. P., Baganoff, F. K., Maeda, Y., Morris, M., Howard, C., Bautz, M. W., & Garmire, G. P. 2004, ApJ, 603, 548
Parmar, A. N., Culhane, J. L., Rapley, C. G., Wolfson, C. J., Acton, L. W., Phillips, K. J. H., & Dennis, B. R. 1984, ApJ, 279, 866
Scargle, J. D. 1998, ApJ, 504, 405
Tokunaga, A. T. 2000, in Allen's Astrophysical Quantities, ed. A. N. Cox (New York: Springer), 143
Vink, J., Kaastra, J. S., & Bleeker, J. A. M. 1997, A&A, 328, 628
Weisskopf, M. C., Brinkman, B., Canizares, C., Garmire, G., Murray, S., & Van Speybroeck, L. P. 2002, PASP, 114, 1